Physica D 473 (2025) 134546

Contents lists available at ScienceDirect

Physica D

journal homepage: www.elsevier.com/locate/physd

Breaking of mirror symmetry reshapes vortices in chiral nematic liquid crystals

Sebastián Echeverría-Alar [a,*], Marcel G. Clerc [b]

[a] Department of Physics, University of California, San Diego, 92093, CA, USA
[b] Departamento de Fisica and Millennium Institute for Research in Optics, Facultad de Ciencias Fisicas y Matematicas, Universidad de Chile, Casilla 487-3, Santiago, Chile

ARTICLE INFO

Communicated by Dmitry Pelinovsky

Keywords:
Nematic liquid crystals
Ginzburg–Landau
Vortices
Chirality

ABSTRACT

Nematic liquid crystals offer a rich playground to explore the nonlinear interaction between light and matter. This richness is significantly expanded when nematic liquid crystals are doped with chiral molecules. In simple words, a favorable twist is introduced at a mesoscopic scale in the system, which is manifested through a characteristic length scale, the helical pitch. A classical controlled experiment to observe the response of chiral nematic liquid crystals to external stimuli, is to fill a liquid crystal cell and apply a continuous electrical current. The aftermath will depend on a balance between the elastic and electric properties of the material, the amplitude and frequency of the electric signal, and the competition between the helical pitch and the cell thickness. Although this balance have been studied experimentally and numerically to some extent, the theoretical side of it has been underexplored. In this work, using weakly nonlinear analysis, we derive from first principles a supercritical Ginzburg–Landau type of equation, enabling us to determine theoretically the intricate balance between physical properties that govern the emergence of some chiral textures in the system. Specifically, we focus on how positive and negative vortex solutions of a real cubic Ginzburg–Landau equation are affected by the presence of chirality. We use numerical simulations to show that +1 vortices undergo isotropic stretching, while -1 vortices experience anisotropic deformation, which can be inferred from the free energy of the system. These deformations are in agreement with previous experimental observations. Additionally, we show that it is possible to break the monotonous spatial profile of positive vortices in the presence of chirality.

1. Introduction

Liquid crystals are a state of matter exhibiting properties of both liquids and solids, and at room temperature they usually exhibit a nematic phase, where their anisotropic constituents, molecules, are characterized by a long-range orientational order, but not a positional one [1,2]. This nematic order is commonly described by a nematic director $\vec{n}$, which accounts for the average orientation of the molecules. Liquid crystals have served as an ideal physical system for studying self-organization in response to diverse external stimuli [3]. In the field of nonlinear optics, experimental setups have been built to leverage the nonlinear response of nematic liquid crystal materials to light. An iconic experiment is the liquid crystal light valve with optical feedback, which has allowed to explore the formation of patterns [4], bistability between localized structures [5], and the localization of spatiotemporal chaos [6], to mention a few. Moreover, the interest in learning how to control localized structures with light has led physicists to propose experimental and theoretical studies based on the unique properties of the nematic liquid crystals. For example, controlling the interplay between diffraction and nonlinearities in this medium have allowed to investigate the interaction and stabilization of optical solitons, or nematicons [7–9]. Recent studies have shown that the nonlinear response of the nematic liquid crystals can be enhanced by doping the system with chiral molecules [10], and thus, breaking the mirror symmetry in the medium [11]. Other theoretical investigations have focused in understanding the role of the nonlocal reorientational dynamics in the localization of beams in a nonlinear optical ring cavity filled with nematic liquid crystal [12], and also in studying the orientational effects of liquid crystals in Fabry–Perot resonators [13].

Although the interaction of nematic liquid crystals with light has received a lot of attention, other type of perturbations can reveal the abundant different phases of this material [3,14]. In particular, a typical experimental configuration is to sandwich a nematic liquid crystal, with negative dielectric anisotropy, between two glasses

* Corresponding author.
E-mail address: secheverriaalar@ucsd.edu (S. Echeverría-Alar).

https://doi.org/10.1016/j.physd.2025.134546
Received 30 October 2024; Received in revised form 22 January 2025; Accepted 24 January 2025
Available online 1 February 2025

coated to enforce a boundary condition such that the equilibrium configuration of the nematic director is uniformly perpendicular to the two glasses (homeotropic anchoring). Then, a sufficiently high electric voltage can be applied in the nematic liquid crystal cell to trigger local reorientations of the nematic order, Fréedericksz transition, generating non-smooth distributions of the nematic director field $\vec{n}(\vec{r})$, where $\vec{r} = (x, y, z)$ is a vector describing position [15]. This texture, which has fascinated the liquid crystal community over decades [16], is called Schlieren and is characterized by displaying disclinations with positive and negatives topological charges [17], which have been also introduced as umbilical defects by Rapini [18], who described these defects in terms of the elastic constants governing the allowed deformations in the nematic phase: splay, bend, and twist [19,20]. Notably, the presence of defects is a transient, which is governed by the minimization of the elastic energy in the system by annihilating pair of defects with different sign through a coarsening process [21–23]. The evolution of these dissipative vortices can be influenced by heterogeneities [24], magnetic fields [25], thermal fluctuations [26], and the frequency of the applied voltage [27–29]. Most importantly for our present work, all of these experimental situations can be fairly well-described with two-dimensional Ginzburg–Landau equations, which are valid in the vicinity of the reorientational instability [30–32]. These equations govern the evolution of a complex field $A(x, y)$ representing the orientation of the 2D projection of the nematic director. The Ginzburg–Landau equations extend well beyond the realm of liquid crystals, in fact, these minimal models arise close to modulational or oscillatory instabilities across different areas of physics and have been extensively studied over the past decades [33–36]. We will be interested in the topological particle-like solutions of real Ginzburg–Landau equations, which are characterized by their $\pm 2\pi$ phase jump surrounding a zero of the complex field A. The sign of this phase singularity, when considering a closed trajectory around it, assigns a topological charge to these solutions. A positive (counterclockwise) jump gives a charge of $+1$ and a negative (clockwise) one a charge of -1.

As we have already mentioned, adding chiral molecules to nematic liquid crystals can modify the properties of the mixture and, as expected, the possible phases and dynamics in the system [1,3,17]. Indeed, the inclusion of chiral dopants can cause a spontaneous twist in the nematic phase [37], resulting in a helical structure of the director $\vec{n}(\vec{r})$. A key signature of this phase is the pitch p, which accounts for the distance needed for the nematic director to complete a 2π rotation. This length scale is the mesoscopic manifestation of the molecular chirality [38]. When subjected to homeotropic boundary conditions, the twisted (wound) phase becomes frustrated and is replaced by a nematic (unwound) phase [39,40]. In this scenario, the twisted phase is known as transitionally invariant configuration (TIC), and it can be recovered by applying a sufficiently high voltage [41,42]. Fig. 1A and B illustrate schematic representations of the experimental setup under consideration and the distribution of the nematic director in the TIC phase, respectively. Similar to the Fréedericksz transition for pure nematics, the bifurcation from the frustrated nematic phase (where all molecules are vertically oriented) into the TIC is mediated by the emergence of dissipative vortices, driven by an annihilation dynamics between umbilical defects affected by chiral effects. Despite systematic explorations of the rich number of topological textures exhibited by chiral nematic liquid crystals [43–47], such as cholesteric fingers and their instabilities [48–52], fewer studies have focused in the study of umbilics under the influence of chiral effects. To our knowledge, there is only one previous experimental work that addresses this issue [53]. In that study, the authors show that defects can undergo an anisotropic elongation and an isotropic shrinking (or expansion), depending on their topological charge. However, there is no systematic quantification of how those changes in shape can be controlled. A pair of phenomenological models have been proposed to study the consequences of chirality in nematic liquid crystals [53,54], suggesting that these effects are governed only by the cholesteric pitch. Nowadays, understanding how chiral effects can be controlled and how they quantitatively affect the shape of vortices could be valuable for patterning light through chiral vortex arrays [55]. In this work, we address theoretically the effects of electrical forcing in frustrated chiral nematic liquid crystals by deriving a supercritical chiral-anisotropic Ginzburg–Landau equation from first principles through a weakly nonlinear analysis. We show how a balance between voltage, geometric frustration and elasticity controls chiral effects in specific experimental scenarios. We numerically investigate the consequences of the mirror symmetry breaking in the spatial structure of positive and negative Ginzburg–Landau vortices, reproducing previous experimental observations. Finally, we give some future perspectives of possible applications of our theory in experiments, and also propose future theoretical directions.

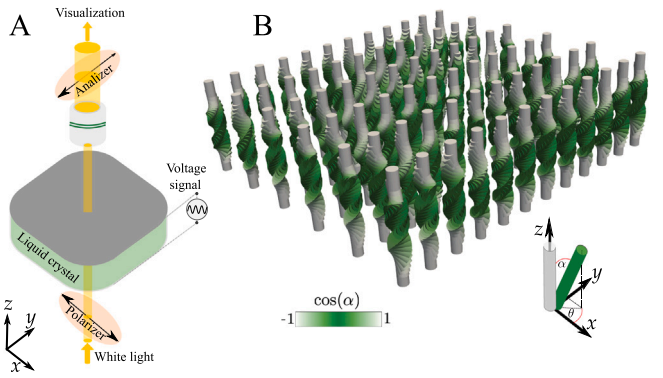

Fig. 1. Experimental setup. (A) Schematic representation of a classic voltage driven experiment, where a chiral nematic liquid crystal, inside a cell treated to induce homeotropic anchoring at their surface, experiences controlled electrical variations. The resulting dynamics can be visualized with polarized optical microscopy techniques. The figure shows a crossed polarizer (polarizer-analizer) configuration. (B) Schematic representation of the director configuration $\vec{n}$ in the TIC phase. The angles α and θ correspond to the tilt angle of the director with respect to the z-axis, and the angle between the x-axis and the projection of $\vec{n}$ in the x-y plane, respectively.

2. Theoretical results

2.1. Dissipative dynamics in chiral nematic liquid crystals

To shed light in the shape of dissipative vortices in frustrated chiral nematic liquid crystals at fixed temperature under the forcing of an electric field, we start from a well-established continuum theory. We assume that in a weakly distorted regime (small spatial variations of $\vec{n}(\vec{r})$), the local properties of the material are the ones of a uniaxial liquid crystal [1]. This assumption allows to write a Frank-Oseen type of free energy for chiral nematics [1–3]

$$\mathcal{F}[\vec{n}, \nabla\vec{n}] = \int \left[\frac{K_1}{2}(\nabla \cdot \vec{n})^2 + \frac{K_2}{2}(\vec{n} \cdot \nabla \times \vec{n} + 2\pi/p)^2 + \frac{K_3}{2}(\vec{n} \times \nabla \times \vec{n})^2 - \epsilon_a(\vec{E} \cdot \vec{n})^2 \right] d\vec{r}, \tag{1}$$

where K_1, K_2, and K_3 are elastic constants associated to the splay, twist, and bend deformation modes, respectively. The cholesteric pitch p needs to be big, compared to a molecular scale l, so the supposition of uniaxiality remains valid [37]. ϵ_a is the dielectric anisotropic constant, which we consider to be negative ($\epsilon_a < 0$), i.e., the chiral nematic liquid crystal molecules will try to be perpendicular to the electric field. The latter is considered to be oriented in the z-direction and is controlled by an external voltage; $\vec{E} = V/d\hat{z}$, where d is the thickness of the cell. The cell is assumed to have a square shape in the x–y plane, with a size $L \gg \{d, p\}$. We have neglected the contribution of saddle-splay deformations in Eq. (1) by assuming that the liquid crystal cell imposes a strong anchoring at its boundaries [56].

To account for the dynamics of the chiral nematic liquid crystal within the cell, we introduce a concrete experimental scenario. We consider the nematic liquid crystal MLC-6609 mixed with the chiral dopant ZLI-811, confined within a cell of thickness $d \leq 10$ μm, and subjected to a voltage amplitude of up to 4 V at a high frequency (>1 kHz). Particularly, previous studies have shown that this material, under such forcing, does not exhibit relevant hydrodynamic effects [57,58], which could be important in other circumstances [59]. Moreover, operating in the high frequency regime should avoid inertial effects, such as electroconvection, charge currents, and material flows [58,60]. Therefore, it is reasonable to assume purely dissipative dynamics when electrical energy is injected into the system [61]. This dynamic behavior can be modeled by a minimization process given by the temporal evolution of the nematic director field

$$\gamma \frac{d\vec{n}}{dt} = -\frac{\delta \mathcal{F}}{\delta \vec{n}} + \vec{n}\left(\vec{n}\cdot\frac{\delta \mathcal{F}}{\delta \vec{n}}\right), \tag{2}$$

where γ is a rotational viscosity constant. The last term ensures the maintenance of the unitary norm $|\vec{n}|^2 = 1$ [61]. Replacing the free energy Eq. (1) into Eq. (2), one gets

$$\begin{aligned}\gamma \frac{d\vec{n}}{dt} &= K_3[\nabla^2\vec{n} - \vec{n}(\vec{n}\cdot\nabla^2\vec{n})] + (K_3 - K_1)[\vec{n}(\vec{n}\cdot\nabla)(\nabla\cdot\vec{n}) - \nabla(\nabla\cdot\vec{n})] \\ &+ (K_2 - K_3)[2(\vec{n}\cdot\nabla\times\vec{n})\{\vec{n}(\vec{n}\cdot\nabla\times\vec{n}) - \nabla\times\vec{n}\} + \vec{n}\times\nabla(\vec{n}\cdot\nabla\times\vec{n})] \\ &+ \frac{4\pi K_2}{p}[-\nabla\times\vec{n} + \vec{n}(\vec{n}\cdot\nabla\times\vec{n})] - \epsilon_a[\vec{n}\cdot\vec{E}(\vec{n}(\vec{n}\cdot\vec{E}) - \vec{E})],\end{aligned} \tag{3}$$

with the boundary conditions $\vec{n} = \hat{z}$ at $z = 0$ and $z = d$ (homeotropic anchoring), and periodic boundary conditions in the lateral directions. The latter is a reasonable assumption given that $L \gg d$.

We begin by analyzing the linear regime of Eq. (3). Particularly, we perturb the frustrated nematic phase $\vec{n}_o = \hat{z}$ with small perturbations of the form $\vec{n} = (n_1, n_2, \sqrt{1 - n_1^2 - n_2^2})$, obtaining

$$\gamma \frac{\partial n_1}{\partial t} = K_3\partial_{zz}n_1 + \frac{4\pi K_2}{p}\partial_z n_2 - \epsilon_a \frac{V^2}{d^2}n_1, \tag{4}$$

$$\gamma \frac{\partial n_2}{\partial t} = K_3\partial_{zz}n_2 - \frac{4\pi K_2}{p}\partial_z n_1 - \epsilon_a \frac{V^2}{d^2}n_2. \tag{5}$$

Notice that the third component of the perturbation was restrained due to the norm conservation. To find the conditions in which the frustrated nematic will bifurcate into the TIC phase, winding/unwinding transition, we introduce the ansatz $n_1 = \alpha_o \cos(fz)\sin(\pi z/d)e^{\sigma t}$ and $n_2 = \alpha_o \sin(fz)\sin(\pi z/d)e^{\sigma t}$ [54,62]. These linear modes satisfy the homeotropic boundary conditions and consider the frustrated rotation, at rate f, induced by the chiral term ($\sim p^{-1}$) inside the liquid crystal cell. α_o is a constant and σ is the linear growth rate of the perturbation. We introduce the ansatz for n_1 and n_2 into Eqs. (4) and (5), set the condition $\sigma = 0$, and get the critical voltage for the reorientational instability $V_c^2 = d^2\left[4\pi K_2 f_c/p - (f_c^2 + \pi^2/d^2)K_3\right]/\epsilon_a$ as a function of the thickness d and the critical frustrated rotation $f_c = 2\pi K_2/pK_3$. A more compact definition for the critical voltage at the bifurcation is

$$V_c = V_f\left(1 - \frac{4K_2^2C^2}{K_3^2}\right)^{1/2}, \tag{6}$$

where $C = d/p$ is the confinement ratio (geometric frustration) and $V_f = \pi\sqrt{K_3/|\epsilon_a|}$ is the Freedericksz voltage [15]. This voltage accounts for the reorientational instability of pure nematic liquid crystals. The voltage-confinement relationship has been derived before through different techniques [3,41,63]. Note that Eq. (6) implies that chirality decreases the voltage necessary to trigger the TIC phase from the nematic. Additionally, the thickness must satisfy $d < K_3 p/2K_2$. This can be understood by thinking that if the thickness of the cell is too large, then, there is no frustration of the chiral phase in the first place. Also, notice that in the limit $p \to \infty$; $V_c \approx V_f$. It is important to highlight that we are assuming that the thickness d is constant for this analysis, and the only bifurcation parameter is the voltage.

2.2. Weakly nonlinear analysis of the winding/unwinding transition

Close to the critical voltage V_c, we perform a weakly nonlinear analysis to find the slow dynamics of the director $\vec{n}(\vec{r}, t)$ near the double critical point. In such nonlinear regime, we need to take into account the $x-y$ dependence of n_1 and n_2. A simple way to consider this spatial dependence near the bifurcation is by introducing the following ansatz for the director field [49,51,54,62]

$$\begin{pmatrix} n_1 \\ n_2 \\ n_3 \end{pmatrix} = \begin{pmatrix} \cos\left(f_c z + \theta\right)\sin\left(\alpha \sin\left(\frac{\pi z}{d}\right)\right) \\ \sin\left(f_c z + \theta\right)\sin\left(\alpha \sin\left(\frac{\pi z}{d}\right)\right) \\ \cos\left(\alpha \sin\left(\frac{\pi z}{d}\right)\right) \end{pmatrix}, \tag{7}$$

where α and θ correspond to the angle tilt of $\vec{n}$ from the z-axis, and the angle between the x-axis and the projection of $\vec{n}$ into the x–y plane, respectively (see Fig. 1B). Both α and θ are slowly varying spatiotemporal variables. In the limit $\alpha \ll 1$, one can introduce the small complex order parameter $A(x, y, t) = \alpha e^{i\theta} = u + iv$ to characterize the behavior of chiral nematic liquid crystals close to the winding/unwinding transition [54]. We can rewrite Eq. (7) as a function of u and v by expanding the components of $\vec{n}$ in the limit $\alpha \ll 1$:

$$\begin{pmatrix} n_1 \\ n_2 \\ n_3 \end{pmatrix} \approx \begin{pmatrix} u\cos\left(f_c z\right)\sin\left(\frac{\pi z}{d}\right) - v\sin\left(f_c z\right)\sin\left(\frac{\pi z}{d}\right) + W_1^{[3]} + \cdots \\ v\cos\left(f_c z\right)\sin\left(\frac{\pi z}{d}\right) + u\sin\left(f_c z\right)\sin\left(\frac{\pi z}{d}\right) + W_2^{[3]} + \cdots \\ 1 - \frac{n_1^2}{2} - \frac{n_2^2}{2} + \cdots \end{pmatrix}, \tag{8}$$

where $\vec{W}^{[3]} = (W_1^{[3]}, W_2^{[3]})$ are higher nonlinear corrections of cubic order and the ellipsis indicates even higher nonlinear corrections. Then, after substituting this ansatz into Eq. (3), we obtain the following linear problem

$$\begin{pmatrix} K_3\partial_{zz} & \frac{4\pi K_2}{p}\partial_z \\ -\frac{4\pi K_2}{p}\partial_z & K_3\partial_{zz} \end{pmatrix}\begin{pmatrix} W_1^{[3]} \\ W_2^{[3]} \end{pmatrix} = \begin{pmatrix} b_1 \\ b_2 \end{pmatrix}, \tag{9}$$

where the 2×2 matrix is a linear operator, $\mathcal{L}$, and the right hand side vector $\vec{b} = (b_1, b_2)$ contains all the other terms coming from Eq. (3). To solve Eq. (9), we need to introduce an inner product to apply a solvability condition, i.e., the linear equation will have solution if and only if $\vec{b}$ is orthogonal to the elements of $Ker\{\mathcal{L}^\dagger\}$. We consider the inner product $\langle\vec{g}|\vec{h}\rangle = \int_0^d \vec{g}\cdot\vec{h}dz$, noting that, under this inner product, the linear operator is self-adjoint, i.e., $\mathcal{L} = \mathcal{L}^\dagger$. The elements of the kernel of the self-adjoint operator are

$$Ker\{\mathcal{L}^\dagger\} = \left\{\begin{pmatrix}\cos(f_c z)\sin(\pi z/d) \\ \sin(f_c z)\sin(\pi z/d)\end{pmatrix}, \begin{pmatrix}\sin(f_c z)\sin(\pi z/d) \\ -\cos(f_c z)\sin(\pi z/d)\end{pmatrix}\right\}. \tag{10}$$

After imposing the two solvability conditions and straightforward calculations, we obtain the amplitude equation

$$\begin{aligned}\frac{\gamma}{2K_2}\partial_t A &= \frac{\pi^2}{2d^2}\left(4K_{23}C^2 - K_{32} - \frac{\epsilon_a V^2}{\pi^2 K_2}\right)A \\ &+ \frac{\pi^2}{4d^2}\left(\frac{3\epsilon_a V^2}{2\pi^2 K_2} - K_{12} + 3\left(2C^2K_{23} - 4C^2K_{23}^2 + \frac{K_{32}}{2}\right)\right) \\ &\times |A|^2 A + \frac{K_{12}+1}{4}\nabla^2 A - \frac{1-K_{12}}{8\pi}\frac{\pi^2\sin(2q)}{2CK_{23} - 8C^3K_{23}^3}\partial_\eta\partial_\eta\bar{A} \\ &+ \frac{4\pi^3}{d}Q(q)(6\pi C + q(3 + K_{12} - 4K_{32}))(A\partial_{\bar{\eta}}A - \bar{A}\partial_\eta A),\end{aligned} \tag{11}$$

where $\partial_\eta = \partial_x + i\partial_y$ is the Wirtinger derivative, $Q(q) = \sin(q)/(q^4 - 10\pi^2q^2 + 9\pi^4)$, $q = 2\pi CK_{23}$, $K_{12} = K_1/K_2$ and $K_{32} = K_3/K_2$. $\bar{A}$ and $\partial_{\bar{\eta}}$ correspond to the complex conjugate of A and ∂_η, respectively. We rescale time $\partial_T = (\gamma d^2/K_2\pi^2)\partial_t$, space $\tilde{\partial}_\eta = (d\sqrt{1+K_{12}}/\sqrt{2}\pi)\partial_\eta$ and the complex field

$$\tilde{A} = \sqrt{\frac{1}{2}\left(K_{12} - \frac{3\epsilon_a V^2}{2\pi^2 K_2} - 3\left(2C^2K_{23} - 4C^2K_{23}^2 + \frac{K_{32}}{2}\right)\right)}A, \tag{12}$$

obtaining the supercritical chiral-anisotropic Ginzburg–Landau equation

$$\partial_T A = \mu A - |A|^2 A + \tilde{\nabla}^2 A - \delta \tilde{\partial}_\eta \tilde{\partial}_\eta \bar{A} + \chi (A \tilde{\partial}_{\bar{\eta}} A - \bar{A} \tilde{\partial}_\eta A), \tag{13}$$

where, for simplicity in the notation, we have redefined $\tilde{A}$ as A. When rescaling the complex field, we have assumed that the scaling factor in Eq. (12) is positive and $\mathcal{O}(1)$. A similar equation, but cubic-quintic, has been derived when frustrated chiral nematic liquid crystals are purely driven by temperature [51,62].

The three parameters introduced in Eq. (13) are: the bifurcation parameter $\mu = 4K_{23}C^2 - K_{32} - \epsilon_a V^2/\pi^2 K_2$, which controls the departure from the critical voltage V_c, the anisotropic parameter

$$\delta = \frac{1 - K_{12}}{1 + K_{12}} \frac{\pi \sin(2q)}{4CK_{23} - 16C^3 K_{23}^3}, \tag{14}$$

and the chiral parameter controlling the breaking of mirror symmetry

$$\chi = \frac{16\pi^2 Q(q)}{\sqrt{1 + K_{12}}} \frac{6\pi C + q(3 + K_{12} - 4K_{32})}{\left(K_{12} - \frac{3\epsilon_a V^2}{2\pi^2 K_2} - 3\left(2C^2 K_{23} - 4C^2 K_{23}^2 + \frac{K_{32}}{2}\right)\right)^{1/2}}. \tag{15}$$

Note that, in the meaningful physical interpretation of our argument, i.e., $0 < d < K_3 p/2K_2$; $0 < q < \pi$. This means that the term $Q(q)$ in Eq. (15) never vanishes. However, the term $\sin(2q)$ in Eq. (14) can vanish at certain confinement, $C = K_{32}/4$, allowing the sign of δ to change as a function of C. We highlight that as Eq. (13) is formally derived from a weakly nonlinear analysis, it obeys an appropriate scaling: $\partial_T \sim \tilde{\nabla}^2 \sim |A|^2 \sim \mu \sim \epsilon$, with ϵ a small parameter ($\ll 1$). Namely, for a small bifurcation parameter, the 2D projection of the director dynamics, Eq. (3), is described by Eq. (13).

2.3. Calculation of the chiral parameter

The expression for the chiral parameter is not straightforward to analyze. Therefore, it is worth to explore different experimental scenarios (see Table 1), particularly varying confinements C and voltages V, which are more easily controlled in experiments, compared to the elastic and electric properties of the material. Fig. 2A shows how χ varies as a function of $C < K_{32}/2$ and V when considering the nematic host MLC-6609. The red solid curve represents Eq. (6) and the gray area indicates the region where $V < V_c$. The white area illustrates the region of parameter where the expression under the square root in Eq. (15) is negative, which means that a quintic nonlinearity will be needed to saturate the instability. It can be seen that chiral effects become strong with increasing confinement and with voltages near the critical curve V_c. Rather than focusing solely in the experimental situation described in the Introduction section, we also checked how the parameter χ behaves when considering the nematic hosts ZLI-2806 and MBBA (see Fig. 2B–C, respectively). Between MLC-6609 and ZLI-2806 there is almost no difference. On the other hand, MBBA exhibits a bigger V_c towards smaller confinements and the white area is bigger. Although, we cannot ensure that hydrodynamic and inertial effects are relevant or not when considering MBBA as a nematic host, the similarities between experimental observations and numerical integrations of Eq. (13), detailed in the next section, are fairly good [53]. Additionally, we illustrate how the chiral parameter behaves when considering a chiral nematic liquid crystal in the one-constant approximation, $K_1 = K_2 = K_3$. Fig. 2D shows that in this approximation the chiral effects persist and the supercritical model is always valid.

It is important to highlight that Eq. (13) breaks the typical phase invariance of the real Ginzburg–Landau equation, $A \to Ae^{i\psi_o}$, with ψ_o an arbitrary phase between 0 and 2π. This symmetry breaking is relevant for determining the possible values of χ. Two specific values of ψ_o are noteworthy: $\psi_o = \pm\pi$, for which the phase transformation $A \to Ae^{i\pm\pi}$ is the same as changing $\chi \to -\chi$. Thus, χ is not restricted to be always positive, as shown in Fig. 2, but it can also be negative.

Eq. (13) is formally valid when $V \to V_c$, when $|C - K_{32}/4| \gg \epsilon$ (except in the one-constant case), and when $\chi \sim \mathcal{O}(1)$ ($\gg \epsilon$). Therefore, in a real experimental situation, the supercritical chiral-anisotropic Ginzburg–Landau equation will be a valuable model to study chiral effects around the critical curve V_c, while imposing confinements sufficiently far from $C = K_{32}/4$, and keeping $\chi \gg \epsilon$. In the following, we explore the chiral effects in the vortex solutions of model Eq. (13) in the one-constant approximation, $\delta = 0$. We have checked that the anisotropic effects, which has been studied before [32], do not play a relevant role in the numerical studies performed in the next section. Specifically, we explore how χ affects the shape of the vortex solutions of the real Ginzburg–Landau equation ($\chi = 0$ and $\delta = 0$).

Table 1
Physical properties of the different nematic liquid crystals (NLC). ϵ_o is the permittivity of free space.

NLC	K_1 (pN)	K_2 (pN)	K_3 (pN)	ϵ_a (F m^{-1})
MLC-6609 [58]	17.2	7.51	17.9	$-3.7\epsilon_o$
ZLI-2806 [58]	14.9	7.9	15.4	$-4.8\epsilon_o$
MBBA [64,65]	6.95	4.5	8.99	$-0.7\epsilon_o$
One-constant	2	2	2	$-0.7\epsilon_o$

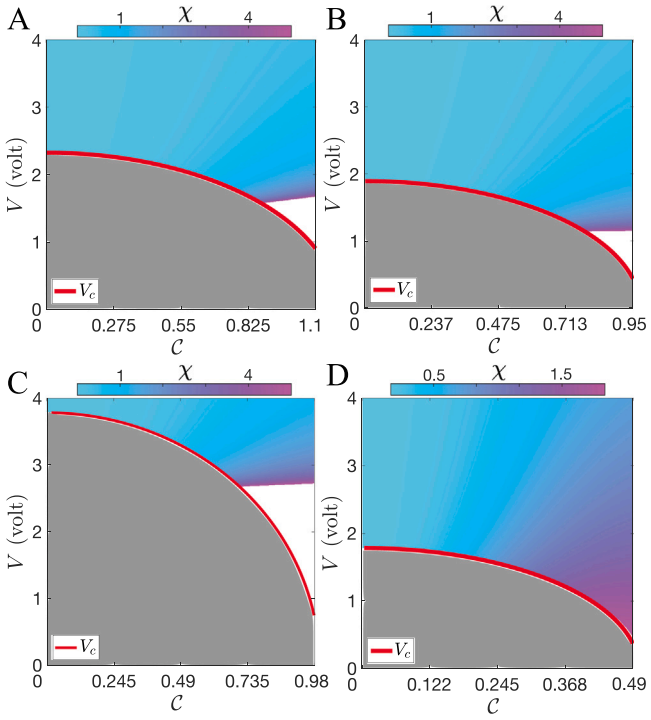

Fig. 2. Phase diagrams in $C - V$ space showing χ for (A) MLC-6609, (B) ZLI-2806, (C) MBBA and (D) the one-constant approximation. The red line indicates the critical voltage Eq. (6). The gray color accounts for the unwound state. The color bar encodes the values of the chiral parameter Eq. (15). The white area illustrates the region of parameters where the expression under the square root in Eq. (12) is negative.

3. Numerical results

To illustrate how the chiral parameter χ influences the vortex solutions in the supercritical chiral-anisotropic Ginzburg–Landau Eq. (13), we perform numerical integrations. We discretize the system with finite differences in space using isotropic stencils in the $x - y$ directions [66], with a spatial step of $\Delta x = 0.25$ (arb. units) and we use non-flux boundary conditions for the amplitude A. These type of boundaries are chosen to enable the study of isolated topological charges. The equations are evolved in time through a Forward Euler method with time step $\Delta t = 0.01$ (arb. units). The numerical procedure to analyze the dissipative vortices is as follows; first, the solution $(u, v) = (0, 0)$ is

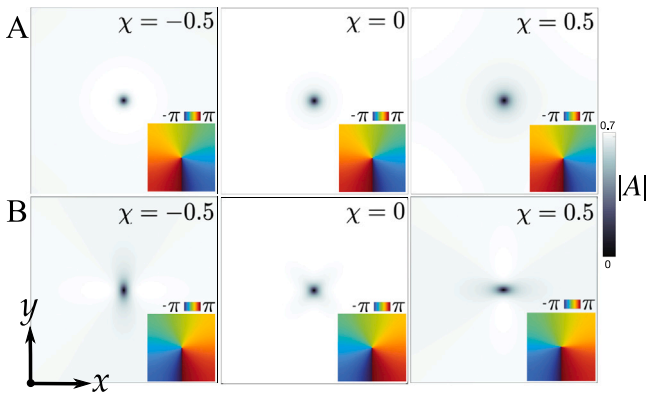

Fig. 3. Modulus fields, $|A|$, for positive (A) and negative (B) vortices for different values of χ. The insets illustrate the phase jump of the vortices. The other parameters are fixed: $\mu = 0.5$, $\delta = 0.0$.

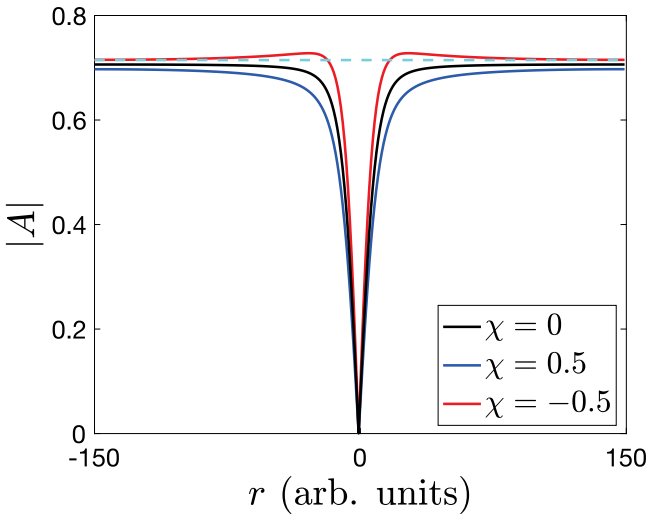

Fig. 4. Chiral effects in positive vortices. Spatial profiles of positive vortices along an arbitrary direction r for different values of χ. The cyan dashed curved represents the asymptotic value ($r \to \infty$) of the modulus in the case $\chi = -0.5$. The other parameters are fixed: $\mu = 0.5$, $\delta = 0.0$.

perturbed with a small amount of Gaussian noise, which will create a few ± 1 vortices when $\mu > 0$. Then, we extract the local u and v fields of positive and negative vortices. Finally, we embed that local structure at the center of a new numerical domain (300×300) and let it evolve for 40 000 timesteps, which is enough to reach steady state ($\partial_t u = \partial_t v = 0$). Fig. 3 shows the modulus field $|A| = \sqrt{u^2 + v^2}$ for positive (top panel) and negative (bottom panel) vortices for three different values of χ, along with their respective phase field $\phi = \tan^{-1}(v, u)$ (see insets in Fig. 3). The latter represents the phase of the complex variable A in its polar representation, $A = |A|e^{i\phi}$, with the origin located at the center of the vortices. The phase is defined in the interval $[-\pi, \pi]$. Qualitatively, it can be seen that the modulus of the positive solutions remain isotropic for either $\chi > 0$ or $\chi < 0$, and their phase is unchanged. However, the vortices with negative charge are drastically affected when chiral terms are present. These vortices undergo an anisotropic stretching of their core, which depending on the sign of χ is either along the y direction or along the x direction in our simulations, respectively. This stretching is accompanied by a modulation in the phase field.

The chiral effect on the vortices with positive charge is simple at first sight, but when looked in detail there is a nontrivial consequence. Fig. 4 illustrates an arbitrary cut, which goes through the center of the vortices for different χ values. When compared to the non-chiral case ($\chi = 0$) (black line), positive values of χ tend to increase the core size of the vortices (blue line), similar to the effect of the anisotropy δ in pure Ginzburg–Landau vortices [32]. However, when $\chi < 0$ (red line), not only there is a compression of the vortex core, but also the monotonous shape of the classical positive Ginzburg–Landau vortex is broken. The value of the new maximum increases with χ. We have also observed a maximum in the amplitude field $|A|$ near the vortex center in localized chiral vortices, which are solutions of the subcritical version of Eq. (13) without electrical forcing [62]. On the other hand, the anisotropic reshaping of the negative vortices can be understood as a simple minimization process. Vortices with negative charge in the Ginzburg–Landau equation possess a hyperbolic structure in the vectorial representation of the complex field A, structure that is maintained when anisotropic effects are considered [32]. This implies that the two-dimensional plane around the negative vortex will be divided into four regions, by a separatrix (see red arrows in Fig. 5A). Most importantly, these four regions can be divided in two sub-regions depending on the direction of rotation of the vector field. When chiral effects are different from zero, the system needs to suppress the two sub-regions with the non-favorable rotation. Fig. 5B–D illustrate different steady state negative vortices with $\chi = -\{0.5, 1, 1.5\}$, respectively, where it can be seen that the anisotropic stretching of the vortex core is intimately related with the collapse of the non-favorable rotations. The insets in these three snapshots represent the chiral energy $\mathcal{F}_\chi = -i\chi|A|^2(\partial_{\bar{\eta}} A - \partial_\eta \bar{A})$ [51,62], and they clearly show how the favorable rotation regions invade the whole square domain. Moreover, the chiral energy allows to visualize that the separatrix curve is deformed near the vortex core. Notice that negative vortices, with or without chiral effects, similarly to positive vortices (see Fig. 4), also smoothly connect the zero solution of A to its asymptotic non-zero value.

4. Conclusions

In this work, motivated from a realistic experimental scenario in liquid crystal research, we have derived a supercritical Ginzburg–Landau type of equation from first principles through a weakly nonlinear analysis, which considers anisotropy, electrical forcing and chirality. Particularly, we have shown how an intricate balance between elastic constants, voltage, cell thickness and helical pitch, controls the chiral term in the Ginzburg–Landau model. Furthermore, Numerical simulations allowed us to illustrate how the breaking of mirror symmetry affects the vortex solutions of the Ginzburg–Landau equation. The positive vortices exhibit an isotropic deformation, capable of stretching or compressing the core of the vortices. The latter is accompanied with the emergence of a non-monotonous behavior in the one-dimensional profile of the modulus field. On the other hand, -1 vortices exhibited an anisotropic stretching of their core due to the chiral effects. The direction of the stretching is dictated by minimizing the spatial extent of the unfavorable rotations around the negative vortices. Although our theoretical formalism simplifies the 3D dynamics by projecting the nematic director onto the 2D plane, we emphasize that the vortex deformations observed numerically closely reproduce previous two-dimensional experimental observations in chiral nematic liquid crystals [53]. Furthermore, our theoretical and numerical results suggest that the deformations are not constrained to a particular chiral nematic liquid crystal.

We think that our findings could help in tailoring experiments in chiral nematic liquid crystals. First, identifying the differences between Schlieren textures in nematic liquid crystals with and without chiral dopants is a complicated task under crossed polarized light microscopy. Our numerical results suggest that these differences should be more clear if the liquid crystal sample is analyzed under circular polarizers, which should give a visualization similar to $|A|$. In a future work,

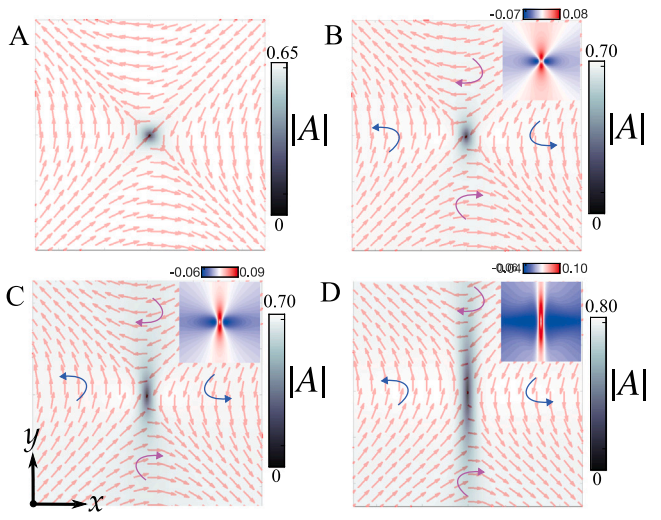

Fig. 5. Effects of chirality in vortices with negative charge. The sequence (A-D) shows the modulus and vectorial representation (red arrows) of A for the values $\chi = -\{0, 0.5, 1, 1.5\}$. The insets in (B-D) accounts for the chiral energy $\mathcal{F}_\chi$. The magenta and blue arrows highlights the division of the hyperbolic vortex in different rotational domains. $\mu = 0.5$, $\delta = 0.0$.

we will conduct this experiment and compare with our current theoretical predictions. Secondly, our model could be used to estimate the cholesteric pitch p, which is not always easy to measure with standard procedures. Finally, the dependence of the chiral parameter on the vortex shapes could motivate experiments to pattern light in chiral nematic liquid crystal cells by spatially modulating χ. This could allow the theoretically informed control of vortex arrays with varying sizes and shapes. On the other hand, future theoretical extensions of the present work could explore the weak anchoring limit where saddle-splay deformations become relevant, as well as investigate how hydrodynamic and inertial effects influence the annihilation dynamics of vortices in chiral nematic liquid crystals.

CRediT authorship contribution statement

Sebastián Echeverría-Alar: Writing – review & editing, Writing – original draft, Software, Methodology, Investigation, Formal analysis, Conceptualization. **Marcel G. Clerc:** Writing – review & editing, Investigation, Conceptualization.

Declaration of competing interest

The authors declare that they have no known competing financial interests or personal relationships that could have appeared to influence the work reported in this paper.

Acknowledgments

We thank Gregorio González-Cortés, Francisco Urbina, Victor Fernández-González, Paulina I. Hidalgo, Jorge Vergara and Vitaly P. Panov for fruitful discussions. S.E.-A. acknowledges the financial support of Beca Chile 74230063. M.G.C. acknowledges the financial support of ANID-Millenium Science Initiative Program-ICN17_012 (MIRO) and FONDECYT 1210353 project.

Data availability

Data will be made available on request.

References

[1] P.G. de Gennes, J. Prost, The Physics of Liquid Crystals, second ed., Clarendon Press, Oxford, UK, 1993.
[2] P.M. Chaikin, T.C. Lubensky, T.A. Witten, Principles of Condensed Matter Physics, vol. 10, Cambridge university press Cambridge, 1995.
[3] P. Oswald, P. Pieranski, Nematic and Cholesteric Liquid Crystals, CRC Press, London, 2005.
[4] S. Residori, Patterns, fronts and structures in a liquid-crystal-light-valve with optical feedback, Phys. Rep. 416 (5–6) (2005) 201–272.
[5] U. Bortolozzo, L. Pastur, P. Ramazza, M. Tlidi, G. Kozyreff, Bistability between different localized structures in nonlinear optics, Phys. Rev. Lett. 93 (25) (2004) 253901.
[6] N. Verschueren, U. Bortolozzo, M.G. Clerc, S. Residori, Spatiotemporal chaotic localized state in liquid crystal light valve experiments with optical feedback, Phys. Rev. Lett. 110 (10) (2013) 104101.
[7] M. Peccianti, K.A. Brzdakiewicz, G. Assanto, Nonlocal spatial soliton interactions in nematic liquid crystals, Opt. Lett. 27 (16) (2002) 1460–1462.
[8] M. Peccianti, C. Conti, G. Assanto, A. De Luca, C. Umeton, Routing of anisotropic spatial solitons and modulational instability in liquid crystals, Nature 432 (7018) (2004) 733–737.
[9] M. Peccianti, G. Assanto, Nematicons, Phys. Rep. 516 (4–5) (2012) 147–208.
[10] G. Poy, A.J. Hess, I.I. Smalyukh, S. Žumer, Chirality-enhanced periodic self-focusing of light in soft birefringent media, Phys. Rev. Lett. 125 (7) (2020) 077801.
[11] W.T.B. Kelvin, The Molecular Tactics of a Crystal, Clarendon Press, 1894.
[12] M. Tlidi, C. Fernandez-Oto, M.G. Clerc, D. Escaff, P. Kockaert, Localized plateau beam resulting from strong nonlocal coupling in a cavity filled by metamaterials and liquid-crystal cells, Phys. Rev. A 92 (5) (2015) 053838.
[13] K. Panajotov, M. Tlidi, Liquid crystal resonator as a nonlinear reflector for passive q-switching and mode locking, Opt. Commun. 549 (2023) 129872.
[14] P. Pieranski, M.H. Godinho, Liquid Crystals: New Perspectives, John Wiley & Sons, 2021.
[15] V. Fréedericksz, V. Zolina, Forces causing the orientation of an anisotropic liquid, Trans. Faraday Soc. 29 (140) (1933) 919–930.
[16] M. Mitov, Liquid-crystal science from 1888 to 1922: Building a revolution, ChemPhysChem 15 (7) (2014) 1245–1250.
[17] I. Dierking, Textures of Liquid Crystals, John Wiley & Sons, 2003.
[18] A. Rapini, Umbilics: static properties and shear-induced displacements, J. Physique 34 (7) (1973) 629–633.
[19] C. Oseen, The theory of liquid crystals, Trans. Faraday Soc. 29 (140) (1933) 883–899.
[20] F.C. Frank, I. liquid crystals, On the theory of liquid crystals, Discuss. Faraday Soc. 25 (1958) 19–28.
[21] T. Nagaya, H. Hotta, H. Orihara, Y. Ishibashi, Observation of annihilation process of disclinations emerging from bubble domains, J. Phys. Soc. Japan 60 (5) (1991) 1572–1578.
[22] L.M. Pismen, Vortices in Nonlinear Fields: From Liquid Crystals to Superfluids, from Non-Equilibrium Patterns to Cosmic Strings, Oxford Science, New York, 1999.
[23] I. Dierking, O. Marshall, J. Wright, N. Bulleid, Annihilation dynamics of umbilical defects in nematic liquid crystals under applied electric fields, Phys. Rev. E—Stat. Nonlinear Soft Matter Phys. 71 (6) (2005) 061709.
[24] V. Zambra, M.G. Clerc, R. Barboza, U. Bortolozzo, S. Residori, Umbilical defect dynamics in an inhomogeneous nematic liquid crystal layer, Phys. Rev. E 101 (6) (2020) 062704.
[25] E. Calisto, M.G. Clerc, V. Zambra, Magnetic field-induced vortex triplet and vortex lattice in a liquid crystal cell, Phys. Rev. Res. 2 (4) (2020) 042026.
[26] E. Aguilera, M.G. Clerc, D. Pinto-Ramos, V. Zambra, Thermal fluctuations induced emergence of umbilical defects in nematic liquid crystal cells, in: Nonequilibrium Thermodynamics and Fluctuation Kinetics: Modern Trends and Open Questions, Springer, 2022, pp. 303–312.
[27] M.G. Clerc, M. Kowalczyk, V. Zambra, Topological transitions in an oscillatory driven liquid crystal cell, Sci. Rep. 10 (1) (2020) 19324.
[28] M.G. Clerc, M. Ferré, R. Gajardo-Pizarro, V. Zambra, Dancing vortices in a driven nematic liquid crystal cell: Theory and experiment, Phys. Rev. E 106 (1) (2022) L012201.
[29] Y. Sasaki, F. Araoka, H. Orihara, Reconfigurable spatially-periodic umbilical defects in nematic liquid crystals enabled by self-organization, J. Phys. D: Appl. Phys. 56 (45) (2023) 453001.
[30] T. Frisch, S. Rica, P. Coullet, J. Gilli, Spiral waves in liquid crystal, Phys. Rev. Lett. 72 (10) (1994) 1471.
[31] T. Frisch, Spiral waves in nematic and cholesteric liquid crystals, Phys. D: Nonlinear Phenom. 84 (3–4) (1995) 601–614.
[32] M.G. Clerc, E. Vidal-Henriquez, J.D. Davila, M. Kowalczyk, Symmetry breaking of nematic umbilical defects through an amplitude equation, Phys. Rev. E 90 (1) (2014) 012507.
[33] M.C. Cross, P.C. Hohenberg, Pattern formation outside of equilibrium, Rev. Modern Phys. 65 (3) (1993) 851.

[34] F. Bethuel, H. Brezis, F. Hélein, et al., Ginzburg-Landau Vortices, Springer, New York, 1994.
[35] I.S. Aranson, L. Kramer, The world of the complex ginzburg-landau equation, Rev. Modern Phys. 74 (1) (2002) 99.
[36] M. Cross, H. Greenside, Pattern Formation and Dynamics in Nonequilibrium Systems, Cambridge University Press, 2009.
[37] A.B. Harris, R.D. Kamien, T.C. Lubensky, Molecular chirality and chiral parameters, Rev. Modern Phys. 71 (5) (1999) 1745.
[38] S. Pieraccini, S. Masiero, A. Ferrarini, G.P. Spada, Chirality transfer across length-scales in nematic liquid crystals: fundamentals and applications, Chem. Soc. Rev. 40 (1) (2011) 258–271.
[39] F. Lequeux, P. Oswald, J. Bechhoefer, Influence of anisotropic elasticity on pattern formation in a cholesteric liquid crystal contained between two plates, Phys. Rev. A 40 (1989) 3974.
[40] C. Long, J.V. Selinger, Explicit demonstration of geometric frustration in chiral liquid crystals, Soft Matter 19 (3) (2023) 519–529.
[41] P. Ribiere, S. Pirkl, P. Oswald, Electric-field-induced phase transitions in frustrated cholesteric liquid crystals of negative dielectric anisotropy, Phys. Rev. A 44 (1991) 8198.
[42] I.I. Smalyukh, B. Senyuk, P. Palffy-Muhoray, O. Lavrentovich, H. Huang, E. Gartland Jr., V. Bodnar, T. Kosa, B. Taheri, Electric-field-induced nematic-cholesteric transition and three-dimensional director structures in homeotropic cells, Phys. Rev. E— Stat. Nonlinear Soft Matter Phys. 72 (6) (2005) 061707.
[43] I.I. Smalyukh, Y. Lansac, N.A. Clark, R.P. Trivedi, Three-dimensional structure and multistable optical switching of triple-twisted particle-like excitations in anisotropic fluids, Nat. Mater. 9 (2) (2010) 139–145.
[44] P.J. Ackerman, I.I. Smalyukh, Diversity of knot solitons in liquid crystals manifested by linking of preimages in torons and hopfions, Phys. Rev. X 7 (1) (2017) 011006.
[45] H.R. Sohn, P.J. Ackerman, T.J. Boyle, G.H. Sheetah, B. Fornberg, I.I. Smalyukh, Dynamics of topological solitons, knotted streamlines, and transport of cargo in liquid crystals, Phys. Rev. E 97 (5) (2018) 052701.
[46] G. Durey, H.R.O. Sohn, P.J. Ackerman, E. Brasselet, I.I. Smalyukh, T. Lopez-Leon, Topological. solitons, Cholesteric fingers and singular defect lines in janus liquid crystal shells, Soft Matter 16 (11) (2020) 2669–2682.
[47] I.I. Smalyukh, Knots and other new topological effects in liquid crystals and colloids, Rep. Progr. Phys. 83 (10) (2020) 106601.
[48] P. Ribiere, P. Oswald, Nucleation and growth of cholesteric fingers under electric field, J. Physique 51 (16) (1990) 1703–1720.
[49] P. Oswald, J. Baudry, S. Pirkl, Static and dynamic properties of cholesteric fingers in electric field, Phys. Rep. 337 (2000) 67.
[50] P.J. Ackerman, R.P. Trivedi, B. Senyuk, J. van de Lagemaat, I.I. Smalyukh, Two-dimensional skyrmions and other solitonic structures in confinement-frustrated chiral nematics, Phys. Rev. E 90 (1) (2014) 012505.
[51] S. Echeverría-Alar, M.G. Clerc, I. Bordeu, Emergence of disordered branching patterns in confined chiral nematic liquid crystals, Proc. Natl. Acad. Sci. 120 (15) (2023) e2221000120.
[52] V. Fernandez-Gonzalez, S. Echeverría-Alar, J. Vergara, P.I. Hidalgo, M.G. Clerc, Topological transition between disordered patterns through heating rate-induced defect emergence, Chaos Solitons Fractals 180 (2024) 114508.
[53] J.M. Gilli, L. Gil, Static and dynamic textures obtained under an electric field in the neighbourhood of the winding transition of a strongly confined cholesteric, Liq. Cryst. 17 (1) (1994) 1–15.
[54] T. Frisch, L. Gil, J.M. Gilli, Two-dimensional landau-de gennes dynamical model for the unwinding transition of a cholesteric liquid crystal, Phys. Rev. E 48 (1993) R4199.
[55] V.P. Panov, J. Yang, L. Migara, H.-J. Yoon, J.-K. Song, Rotation-time symmetry breaking in frustrated chiral nematic driven by a pulse-train waveform, Phys. Rev. Lett. 129 (11) (2022) 117801.
[56] G. Crawford, D.W. Allender, J. Doane, Surface elastic and molecular-anchoring properties of nematic liquid crystals confined to cylindrical cavities, Phys. Rev. A 45 (12) (1992) 8693.
[57] P.J. Vanbrabant, J. Beeckman, K. Neyts, R. James, F.A. Fernandez, Effect of material properties on reverse flow in nematic liquid crystal devices with homeotropic alignment, Appl. Phys. Lett. 95 (15) (2009).
[58] P.J. Ackerman, T. Boyle, I.I. Smalyukh, Squirming motion of baby skyrmions in nematic fluids, Nat. Commun. 8 (1) (2017) 673.
[59] T.C. Lubensky, Hydrodynamics of cholesteric liquid crystals, Phys. Rev. A 6 (1) (1972) 452.
[60] M.G. Clerc, R. Gajardo-Pizarro, Nullclines entanglement induced topological transitions in driven liquid crystal cells, Chaos Solitons Fractals 188 (2024) 115447.
[61] S. Chandrasekhar, Liquid Crystals, Cambridge University Press, Cambridge, UK, 1992.
[62] M.G. Clerc, G. González-Cortés, S. Echeverría-Alar, Localized dissipative vortices in chiral nematic liquid crystal cells, Phys. Rev. Res. vol. 4 (2022) L022021.
[63] E. Gartland, H. Huang, O. Lavrentovich, P. Palffy-Muhoray, I. Smalyukh, T. Kosa, B. Taheri, Electric-field induced transitions in a cholesteric liquid-crystal film with negative dielectric anisotropy, J. Comput. Theor. Nanosci. 7 (4) (2010) 709–725.
[64] G. Porte, J. Jadot, A phase transition-like instability in static samples of twisted nematic liquid crystal when the surfaces induce tilted alignments, J. Physique 39 (2) (1978) 213–223.
[65] H.L. Ong, Optically induced freedericksz transition and bistability in a nematic liquid crystal, Phys. Rev. A 28 (4) (1983) 2393.
[66] A. Kumar, Isotropic finite-differences, J. Comput. Phys. 201 (1) (2004) 109–118.